

**IMPERIAL COLLEGE LONDON**

Faculty of Engineering

*Department of Civil and Environmental Engineering*

---

**Investigation of recoverable negative stiffness  
lattice structures**

---

**Jiachi Yang**

2020-2021

## DECLARATION OF OWN WORK

**Declaration:**

This submission is my own work. Any quotation from, or description of, the work of others is acknowledged herein by reference to the sources, whether published or unpublished.

Signature :           Jiachi Yang

## *Abstract*

The development in additive manufacturing, namely 3D printing, enables the design and fabrication of lattice structures in complicated forms. This research numerically explores mechanical behaviours of recoverable negative stiffness steel lattices which are used as sacrificial structures for the aim of impact or blast isolation. A sacrificial structure normally contains an equilibrium path consisted of a high initial stiffness range and a practically zero post-buckling stiffness range. The lattice structures studied in this research, additionally incorporates a recoverable feature. With deliberate utilization of snap-through instability at unit cell level, sequential buckling behaviour could be harvested at lattice level. It has been shown that the sequential buckling property of lattices successfully maintains a practically constant level of force transferred from sacrificial structure to main structure. An estimated 70 - 85% of recovery is predicted for the investigated lattices.

### **Keywords**

structural isolation, unit cell, lattice structure, finite element modelling, snap-through, sequential buckling, recoverability

## Contents

Abstract .....	1
Chapter 1 INTRODUCTION .....	2
1.1 Background and outline.....	3
1.2 Snap-through buckling and sequential buckling.....	5
1.3 Recoverable lattice structure .....	6
1.4 Material .....	6
Chapter 2 UNIT CELLS.....	7
2.1 Introduction .....	7
2.2 Bare arrowhead unit cell (UC) .....	7
2.3 Arrowhead unit cell with internal struts (UCI).....	14
Chapter 3 LATTICE.....	21
3.1 Introduction .....	22
3.2 Finite Element Modelling of Lattice .....	23
3.3 ‘Lattice Effect’ .....	23
3.4 Lattice with sequential buckling behaviour .....	25
Chapter 4 CONCLUSION and RECOMMENDATION.....	28
References .....	30

# *Chapter 1*

## **INTRODUCTION**

### **1.1 Background and outline**

Conventionally, ‘instability’ is a hostile word to structural engineers as it had been regarded as the green light to numerous structural failures and disasters (Bažant, 2000). However, the progression in nonlinear mechanics has gained access to a new engineering field where structural instability is harnessed for novel applications (Reis, 2015). Hu and Burgueño (2015) points out that one category of buckling-induced application is energy-related such as isolator and absorber. The engineering exploitation of structural instability has been significantly facilitated by the rapid development in metal additive manufacturing which allows metal material to be jointed in free form (Frazier, 2014). Lattice structure, sometimes referred to as metamaterial, is a representative output of additive manufacturing technique (Großmann et al., 2019).

This research is a numerical investigation of a recoverable negative stiffness steel lattice structure working as a sacrificial structure for impact or blast isolation. Being a line of protection for the main isolated structure, a sacrificial structure should play two roles as an energy absorber and a load threshold, which prevents the propagation of excessive energy or force in main structure (Wadee, Phillips & Bekele, 2020). A structural model which satisfies those two requirements, along with its typical load-displacement response, is presented in **Figure 1.1 (a)** and **(b)** (Carrella, Brennan & Waters, 2006:

p.679). The quasi-zero stiffness range in **Figure 1.1 (b)** acts as a load threshold because within this range the increase in displacement will result in no increase in load transferred from sacrificial structure to main structure. Elongating this quasi-zero stiffness range is of prior interest by researchers as the zero-stiffness nature is perfectly efficient for energy absorption. Lattice structure, with its great reputation of large deformation capability, seems to be a solution to meet this objective. McKown et al. (2007) experimentally studied the quasi-static response of a 3D-printed stainless-steel lattice with octahedral cells and obtained a relatively long quasi-zero stiffness range. Wadley et al. (2007) also met that objective by investigating a multi-layer stainless-steel lattice structure with pyramidal cells, sequential buckling behaviour was observed under quasi-static loading experiment. However, the lattices studied in these works are irrecoverable and crushed during experiment. Inspired by previous works, this research focuses on designing a sacrificial lattice structure with sequential buckling behaviour as well as a recoverable feature.

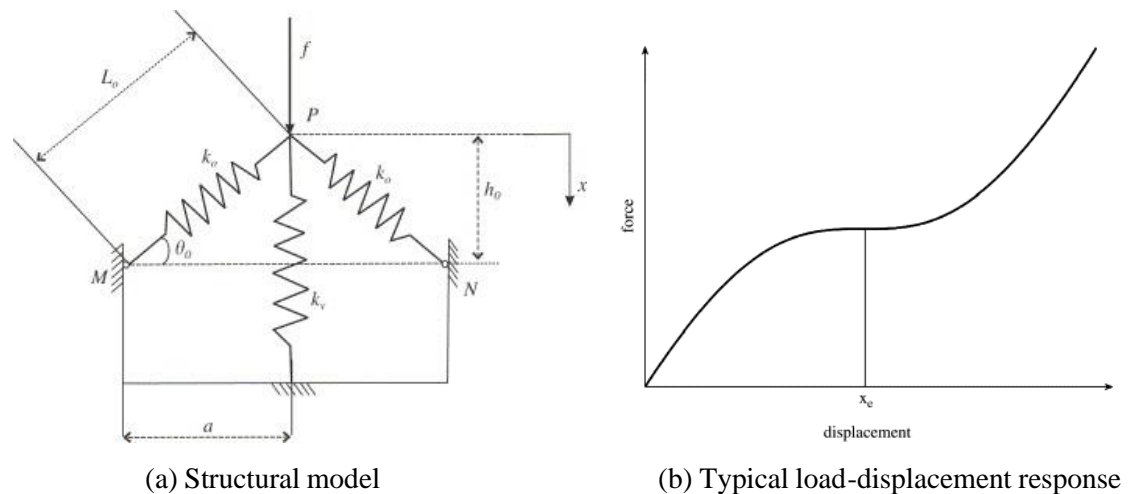


**Figure 1.1** Structural model and load-displacement response of isolator (Carrella, Brennan & Waters, 2006: p.679)

Paper content is organized in a part-to-whole order from unit cell level to lattice level. The second chapter of this study aims at obtaining snap-through behaviour as well as high recoverability from arrowhead unit cells. The snap-through behaviour of unit cells

is then exploited in the third chapter to harvest sequential buckling behaviour from lattice structures.

## 1.2 Snap-through buckling and sequential buckling

The most renowned example of snap-through buckling is the three-hinge von-Mises truss. Similar snap buckling behaviour is also observed in fix-ended toggle frame (Champneys et al., 2019), fix-ended curved beam (Qiu, Lang & Slocum, 2004) and hexagonal lattice cell (Gibson and Ashby, 1999). Snap-through buckling is inherently bi-stable as it involves a stable pre-buckling stage (a), a destabilization negative stiffness post-buckling stage (b) and a restabilization stage (c) (See **Figure 1.2**).

Sequential buckling could be described as a series of destabilization and restabilization process which has been observed in the post-buckling range of cylindrical shells (Hunt et al, 1999), I-section beams (Wadee & Gardner, 2012), I-section struts (Wadee & Li, 2014) and stiffened plates (Wadee & Farsi, 2014). A simple illustration of sequential buckling equilibrium path is shown in **Figure 1.3**.

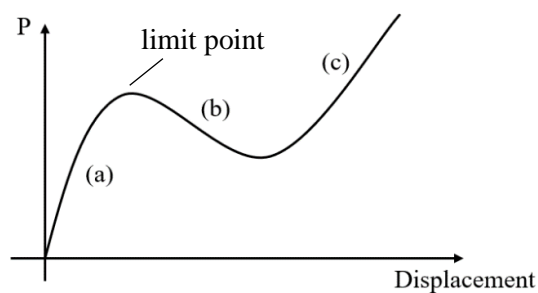


**Figure 1.2** Illustration of snap-through behaviour



**Figure 1.3** Illustration of sequential buckling behaviour

As sequential buckling could be decomposed into a series of destabilization and restabilization process which corresponds to the nature of snap buckling, an inspiration

is such that the sequential buckling of lattice structure could be originated from the snap-buckling of lattice layer in a sequential manner.

### **1.3 Recoverable lattice structure**

Recoverable lattice has been a novel research topic in recent years (Großmann et al., 2019) for its reusable and sustainable feature. Previous studies on recoverable lattice generally adopted super-elastic material or shape memory material. Hatamleh et al. (2021) experimentally studied the structural performance of a 3D-printed rubber sandwich lattice structure under compressive fatigue and achieved full recovery. Liquid metal lattices compressed under 20 °C were demonstrated to exhibit nearly full recovery when the lattices were heated up to 93 °C due to shape memory effect of material (Deng, Nguyen & Zhang, 2020). Cheng et al. (2021) reported that carbon fibre reinforced honeycomb lattice has an approximately 87% recovery under low voltage electrical excitation. However, there is still a research blank in recoverable lattice employing traditional building material such as steel, which introduces the main topic of this research.

### **1.4 Material**

Material employed in this study is stainless-steel powder for additive manufacturing. Detailed material properties can be referred to previous work by Zhang et al. (2021). Important material properties such as Young's modulus, 0.2% proof stress and ultimate strain are taken as 181GPa, 784MPa and 6.3% respectively in this research.

## *Chapter 2*

### UNIT CELLS

#### 2.1 Introduction

A lattice structure is composed of inter-jointed unit cells of which the mechanical behaviours will further imply the overall structural performance of lattices. This section will start from investigating the properties of bare unit cells, namely unit cells without internal struts (denoted as UC), and then seeking for possible structural configurations of unit cells with internal struts (denoted as UCI) to obtain the aforementioned snap-through behaviour.

#### 2.2 Bare arrowhead unit cell (UC)

##### 2.2.1 Geometry, boundary conditions and cross-section

Geometry and boundary conditions of UC are presented in **Figure 2.1**. Geometric parameters are such that  $\alpha$  is the inclination angle of upper beams,  $\beta$  is the inclination angle of lower beams,  $h$  and  $b$  are height and width,  $d$  is the protruding distance of lower beams, namely the vertical distance between node A and node C (or D). UC is under compression in vertical direction with a pinned support at node B and a roller support at node A. Upper and lower beams are both assigned with circular cross-section with radius of  $r_1$  and  $r_2$  respectively.

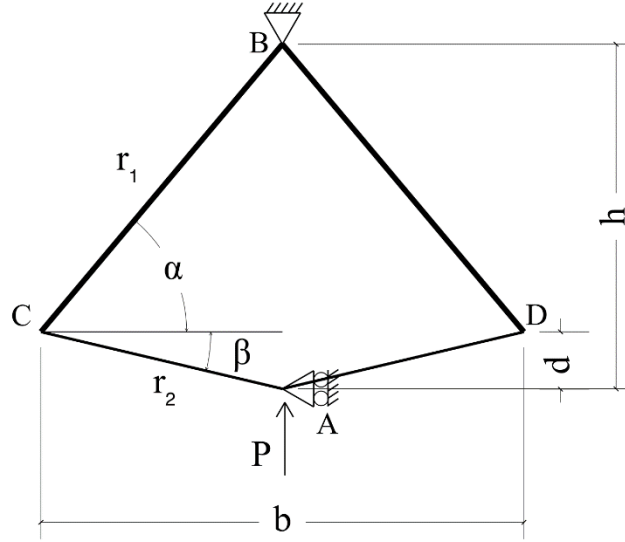


**Figure 2.1** Geometry, boundary conditions and cross-section

### 2.2.2 Loading

As recoverability is of particular interest in this research, a 2-step load-unload procedure needs to be applied such that the percentage of recovery can be examined. **Figure 2.2** illustrates the loading procedure including a load step in which node A is forced to displace  $2d$  and a following unload step.  $2d$  is named as design ultimate displacement that is not expected to be exceeded in normal conditions in practice, because deformation beyond this limit will be disadvantageous to the recoverability. It should be noted that a maximum displacement of  $2d$  should be able to capture, if there is, the snap-through behaviour of UCs. In **Figure 2.2**,  $\delta$  is the vertical displacement of node A and  $\delta^R$  is the residual displacement of node A after unloading. The recoverability of UC is measured by percentage of recovery which is defined as:

$$p_r = \left(1 - \frac{\delta^R}{2d}\right) \times 100\% \quad (2.1)$$

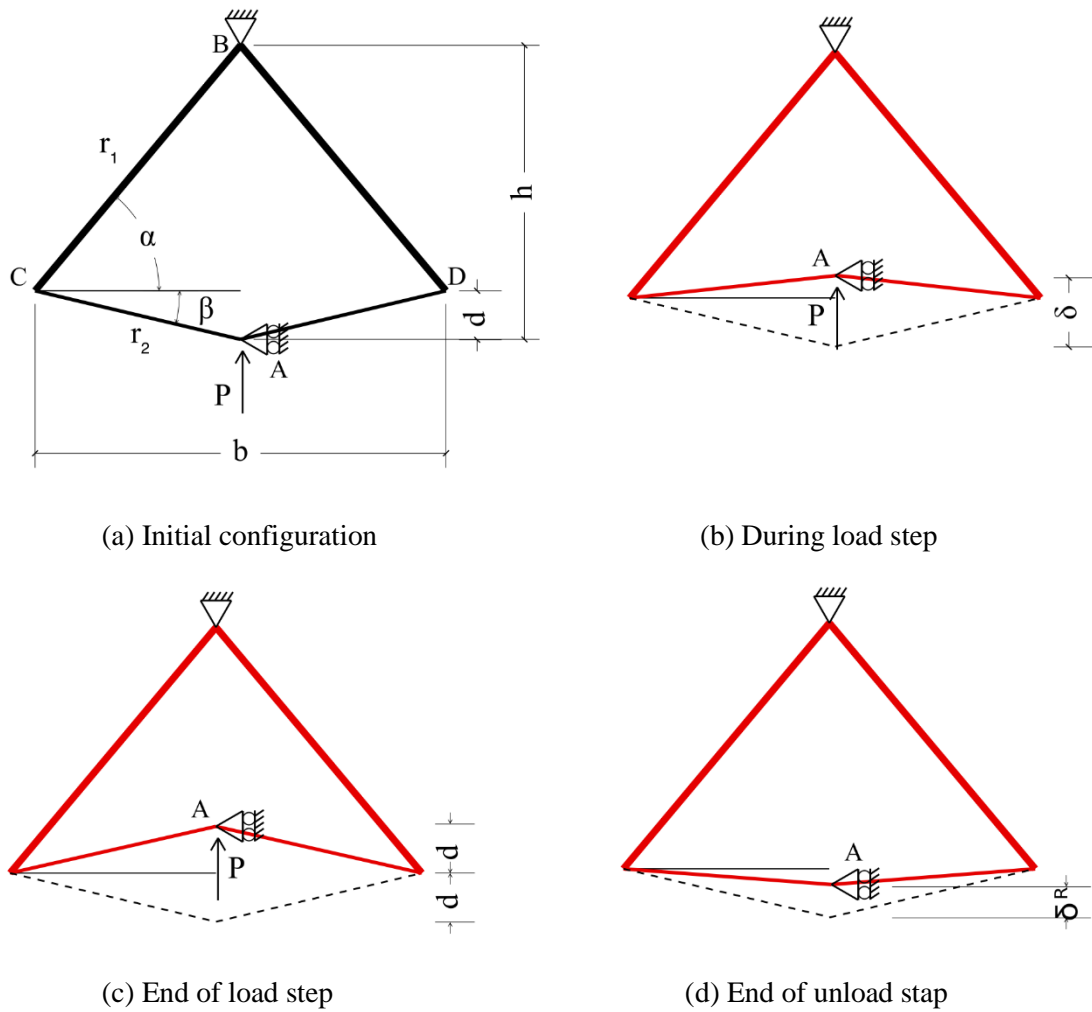


**Figure 2.2** Illustration of loading procedure

### 2.2.3 Finite element modelling

Commercial software Abaqus (2020) is used for finite element (FE) modelling. UCs are modelled in 2D planar space where upper and lower beams are assigned with beam elements. Prior study (Wadee et al., 2010) has indicated that Quadratic Timoshenko beam element (B22) attains a satisfied level of accuracy for modelling deformation of beams in arrowhead unit cells. The load and unload steps described in last section are defined in General Static procedure as General Static procedure allows multiple steps to be defined in sequence. Displacement control is adopted in load step where a tabular vertical displacement from 0 to  $2d$  with a fixed interval of  $0.02d$  is applied at node A.

### 2.2.4 Method

In order to learn the effects of geometric and cross-sectional parameters on the mechanical behaviour of UCs, a set of comparative study is conducted. Except from investigating direct dimensional parameters such as  $\alpha$  and  $r_1$ , two indirect parameters –  $\gamma_a$  (the ratio between  $\beta$ ,  $\alpha$ ) and  $\gamma_r$  (the ratio between  $r_1$ ,  $r_2$ ) – are chosen to represent the changes in geometry and cross-section. **Table 2.1** lists four groups of UCs which are divided by four magnitudes of  $\gamma_a$  while within each group  $\gamma_r$  changes from 1 to 4. Therefore, the effects of  $\gamma_a$  and  $\gamma_r$  can be learned by horizontal comparison across groups and vertical comparison within each group respectively. For all UCs in **Table 2.1**,  $\alpha$ ,  $b$ ,  $r_2$  are set as  $50^\circ$ , 200 mm and 2 mm.

**Table 2.1** Parameters of UCs

Group	UC	$\gamma_a$	$\beta$	$\gamma_r$	$r_1$ (mm)	$2d/h$
1	UC 1-1	1/20	2.5	1	2	0.071
	UC 1-2			2	4	
	UC 1-3			3	6	
	UC 1-4			4	8	
2	UC 2-1	1/10	5.0	1	2	0.137
	UC 2-2			2	4	
	UC 2-3			3	6	
	UC 2-4			4	8	
3	UC 3-1	3/20	7.5	1	2	0.199
	UC 3-2			2	4	
	UC 3-3			3	6	
	UC 3-4			4	8	
4	UC 4-1	1/5	10.0	1	2	0.258
	UC 4-2			2	4	
	UC 4-3			3	6	
	UC 4-4			4	8	

### 2.2.5 Numerical results and findings

Equilibrium paths (with loading and unloading parts) and  $p_r$  of UCs are shown in **Figure 2.3** and **Table 2.2**.

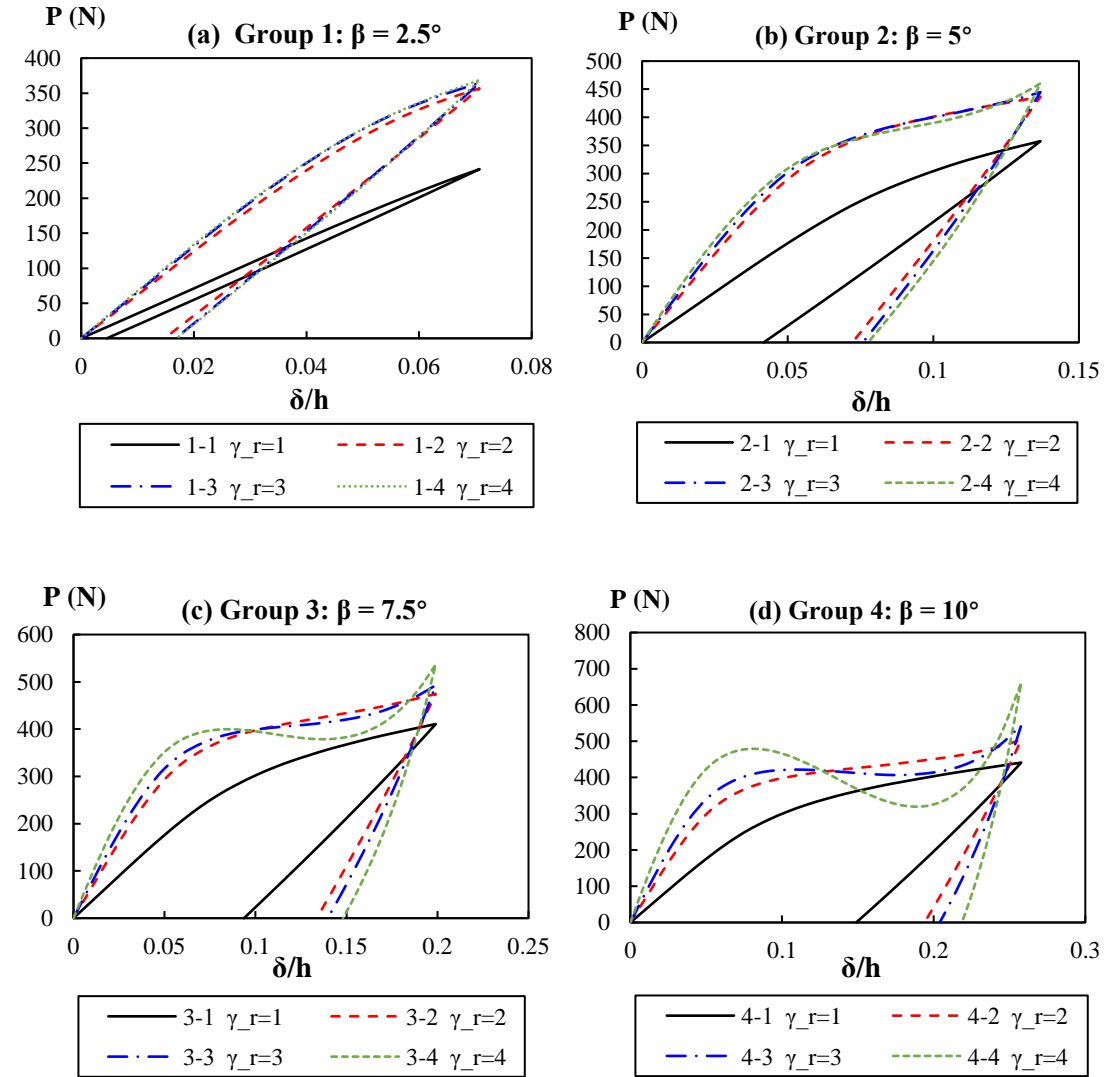


**Figure 2.3** Equilibrium paths of UCs in Table 2.1

**Table 2.2**  $p_r$  of UCs in Table 2.1

UC	1-1	1-2	1-3	1-4	2-1	2-2	2-3	2-4
$p_r$ (%)	93.57	79.10	76.32	76.09	69.49	47.20	44.57	43.31
UC	3-1	3-2	3-3	3-4	4-1	4-2	4-3	4-4
$p_r$ (%)	52.96	32.88	29.80	25.63	42.23	24.76	20.87	15.20

One important finding from **Figure 2.3** is that snap-through behaviour is only observed in UC 3-4, UC 4-3 and UC 4-4. The equilibrium paths of these three UCs are particularly picked from **Figure 2.3** and then plotted in **Figure 2.4** along with deformation shapes corresponding to critical points.

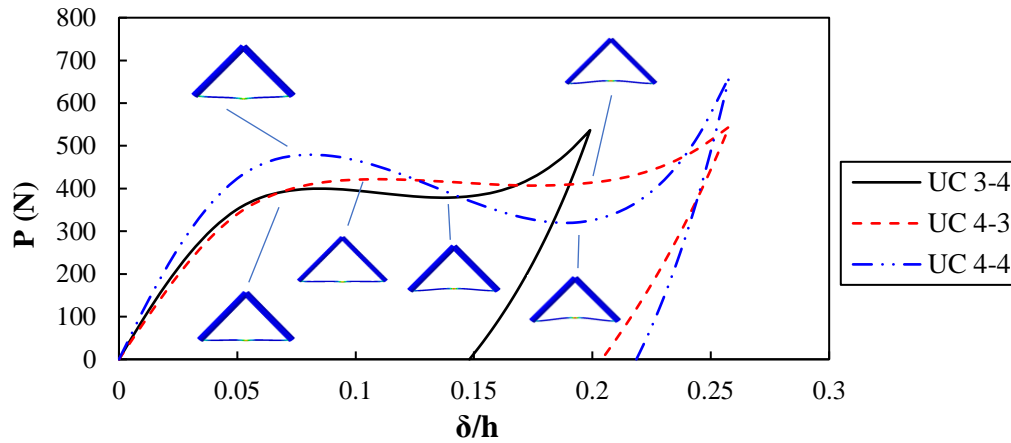


**Figure 2.4** Equilibrium paths of UCs exhibiting snap-through behaviour

An intuitive conclusion is that by increasing  $\gamma_r$  and  $\gamma_a$  simultaneously, snap-through behaviour will somehow be triggered in UC. The underlying reason of this phenomena lays in the interaction between bending and membrane actions: As node A is loaded upwards, lower beams will bend to adapt the resultant deformation and meanwhile push upper beams to expand laterally, which results in a combination of bending and membrane actions. **Figure 2.5** is a free body cut of lower beam AC.  $F_x$  is the horizontal component of force vector on cross-section C, which is used to approximately represent the membrane action.

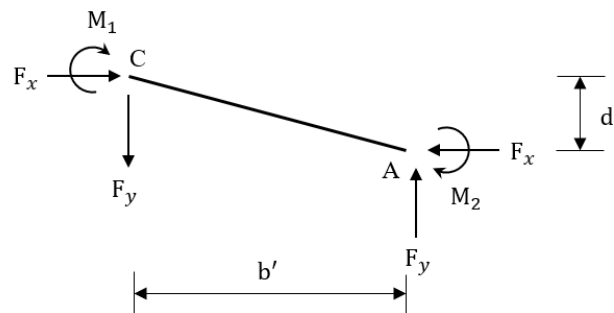


**Figure 2.5** Free body cut of beam AC

For all equilibrium conditions during loading and unloading, we have:

$$F_x \cdot d' + (M_1 + M_2) = F_y \cdot b' \quad (2.2)$$

$$F_y = \frac{(F_x \cdot d')}{b'} + \frac{(M_1 + M_2)}{b'} \quad (2.3)$$

where  $d' = d - \delta$ ,  $b'$  is approximately taken as 100mm for all equilibrium conditions.  $F_y$  is shown to be shared by membrane effect and bending effect represented by the first and second term at right hand side of **Equation 2.3**. **Figure 2.6** shows equilibrium paths of UC 4-2, UC 4-3 and UC 4-4 along with the share of load response by membrane effect and bending effect calculated based on **Equation 2.3**.

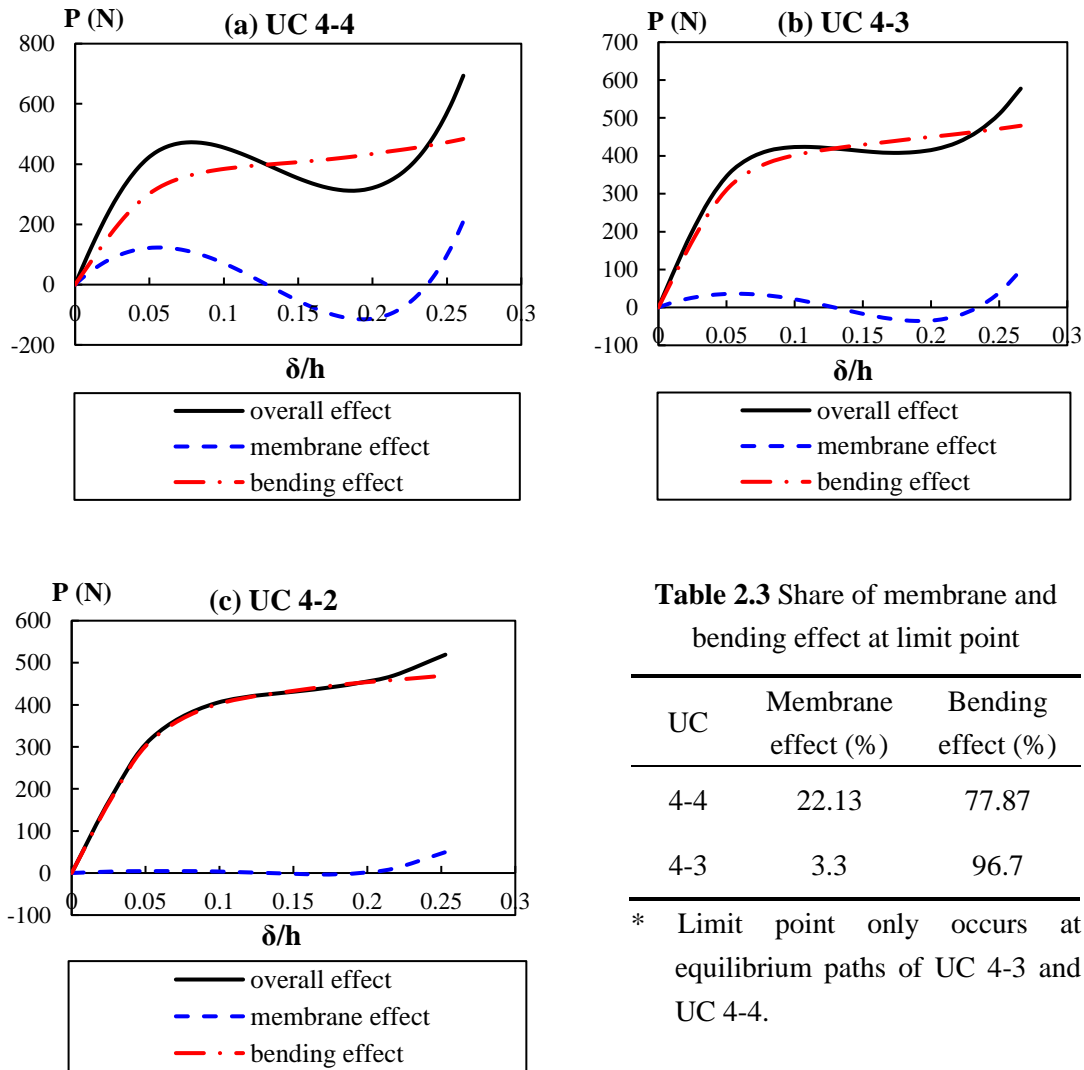


**Figure 2.6** Membrane and bending effect of UC 4-4, UC 4-3 and UC 4-2

It is seen from **Figure 2.6** that the membrane effect of all three UCIs displays snap-through behaviour with that of UC 4-4 the most obvious and that of UC 4-2 very insignificant. Unlike membrane effect, load shared by bending effect exhibits an approximately bi-linear shape which is a result of material yielding at node C and A where critically large deformation is observed. Material yielding at nodal area dramatically slows down the increase of bending effect after  $\delta/h = 0.05$ .

Occurrence of limit point depends on two factors: (a) large  $\gamma_r$ , which leads to more significant membrane effect as upper beams become stiffer; (b) yielding at node C(D) and A, which will rapidly slow down the increase of bending effect, a limit point will appear when the increase of bending effect fails to counteract the decrease of membrane effect.

However, extensive yielding at nodes in turn results in low  $p_r$  (e.g., 15.20% for UC 4-4 and 20.87% for UC 4-3), which indicates that snap-through behaviour and high recoverability cannot co-exist with simple bare arrowhead geometry. Thus, more complex geometry should be explored, which leads to next section.

### **2.3 Arrowhead unit cell with internal struts (UCI)**

In Section 2.2, it has been shown that UCs with same radius of cross-section for upper and lower beams ( $\gamma_r = 1$ ) as well as low  $\gamma_a$  will yield high percentage of recovery, such as UC 1-1 and UC 2-1. Nevertheless, their equilibrium paths are approximate to linear which is of little use for structural isolation. This section seeks for possible ways of adding internal struts in UCs to take advantage of strut buckling, and finally harvests snap-through behaviour and high  $p_r$  simultaneously. Further investigation demonstrated that the equilibrium paths of UCIs are tailorable by designing geometric and cross-sectional parameters.

### 2.3.1 Geometry, boundary conditions and cross-section

Two possible arrangements of internal strut(s) are proposed as shown in **Figure 2.7**. Configuration 1 adopts a vertical middle strut; Configuration 2 incorporates two inclined struts with one end at node A and another end supported at somewhere in the top half of upper beams. In **Figure 2.7**,  $r$  is the radius of external beams,  $r_i$  is the radius of internal strut,  $\gamma_h$  defines the position of the top end of internal strut in Configuration 2, other notations and boundary conditions remain the same as they are in **Figure 2.1**.

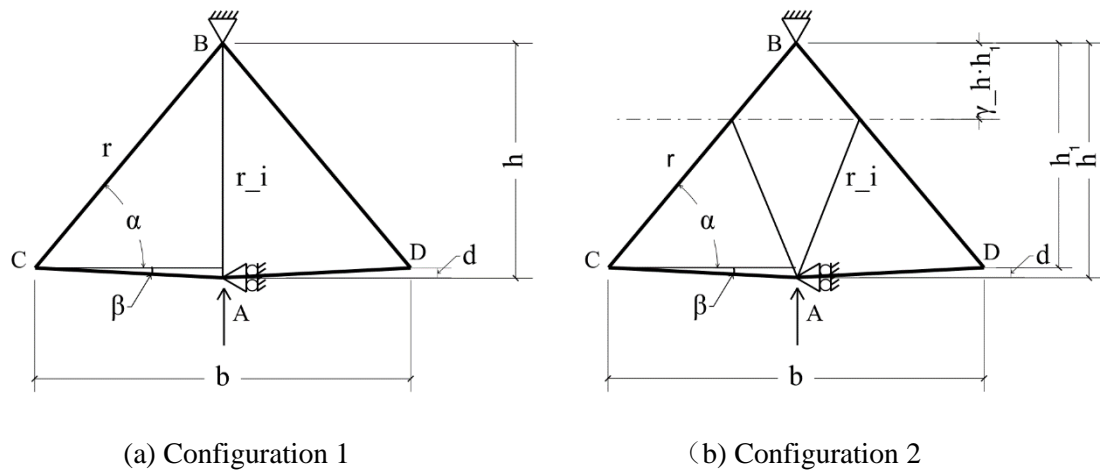


**Figure 2.7** Geometry, boundary conditions and cross-section

### 2.3.2 Loading

The loading procedure are very same as that for UCs (See **Figure 2.2**). Notations in **Figure 2.2** such as  $\delta$  and  $\delta^R$  also apply in this section. As a reminder,  $\delta$  represents the vertical displacement of node A while  $\delta^R$  is the residual vertical displacement of node A after unloading.

### 2.3.3 Finite Element Modelling

FE modelling of UCIs are basically the same as that for UC except from the setting of loading. The loading approach is still defined in Static General procedure, however,

though Static General method enables the calculation of  $p_r$ , it will lose accuracy in terms of capturing buckling load. Therefore, Static General method is not suitable for imperfection sensitivity study. Thus, Static Riks method, which is specifically used for solving limit point and post-buckling problems (Riks, 1979), is employed in imperfection sensitivity study to avoid excessive errors.

### 2.3.4 Method

In order to compare the two configurations, a comparative study is conducted on 10 UCIs listed in **Table 2.4**. The 10 UCIs are grouped by their employed configuration and for all UCIs,  $\alpha$ ,  $\gamma_h$ ,  $r$ ,  $\gamma_a$ ,  $b$  are set as  $50^\circ$ ,  $1/3$ , 2 mm,  $1/20$  and 200 mm respectively. The corresponding values of  $\beta$  and  $2d/h$  are  $2.5^\circ$  and 0.07. The first part of this comparative study includes the comparison of equilibrium paths and recoverability while the second part compares imperfection sensitivity of the two configurations. This study helps examine the suitability of the two configurations and also looks into the effect of  $r_i$  on structural performance.

**Table 2.4** Parameter of UCIs

Group	UCI	$r_i$ (mm)
Configuration 1	UCI 1-1	0.60
	UCI 1-2	0.70
	UCI 1-3	0.80
	UCI 1-4	0.90
	UCI 1-5	1.00
Configuration 2	UCI 2-1	0.60
	UCI 2-2	0.65
	UCI 2-3	0.70
	UCI 2-4	0.75
	UCI 2-5	0.80

### 2.3.5 Numerical results and findings

#### 2.3.5.1 Equilibrium paths and recoverability

The equilibrium paths of UCIs in Group 1 and Group 2 are shown in **Figure 2.8**.  $p_r$  of all UCIs are listed in **Table 2.5**.

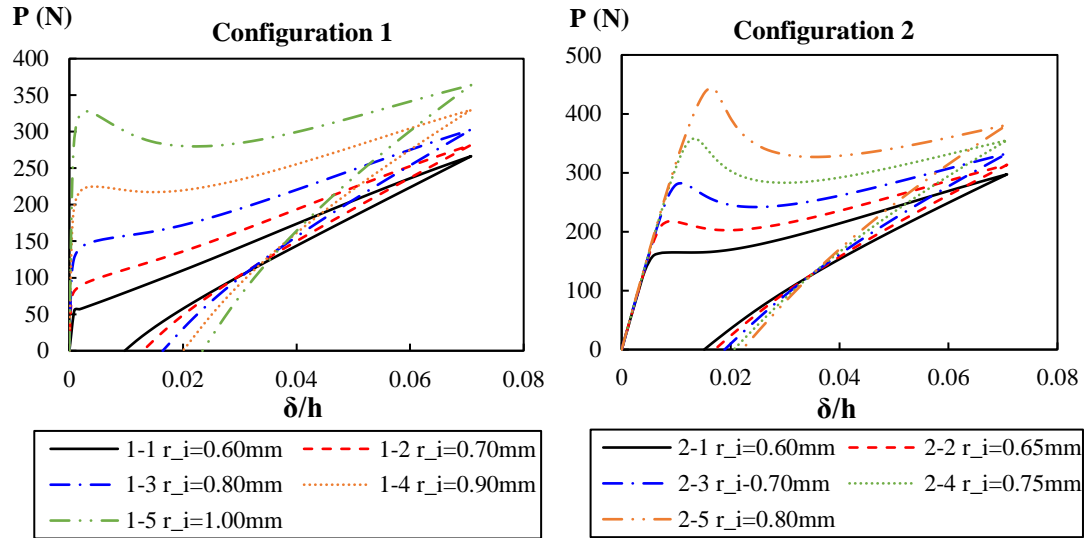


**Figure 2.8** Equilibrium paths of UCIs

**Table 2.5**  $p_r$  of UCIs in Table 2.3

UCI	1-1	1-2	1-3	1-4	1-5
$p_r(\%)$	86.27	81.69	76.77	71.74	66.93
UCI	2-1	2-2	2-3	2-4	2-5
$p_r(\%)$	78.58	75.86	73.30	70.90	68.73

The equilibrium paths in **Figure 2.8** can be categorized into two types: the first type is observed in UCIs with relatively thin internal strut(s) such as UCI 1-1, UCI 1-2, UCI 1-3 and UCI 2-1, which contains a high pre-buckling stiffness followed by a lower positive post-buckling stiffness; the second type is observed in UCIs with relatively thick internal strut(s) such as UCI 1-4, UCI 1-5, UCI 2-2, UCI 2-3, UCI 2-4 and UCI 2-5, which contains the destabilization and restabilization feature, although in UCI 1-4

and UCI 2-2 that destabilization feature is insignificant as the negative stiffness range is nearly flat. In conclusion, snap-through behaviour can be obtained in both configurations by increasing the radius, or in other words, reducing the slenderness of internal strut(s).

The formation mechanism of snap-through behaviour is interpreted as following: A UCI can be decomposed into two constituent parts – internal strut(s) and external beams – with each part making its own contribution to the overall load resistance. Take UCI 1-5 for example, **Figure 2.9** plots its equilibrium path along with the share of load resisted by internal struts and external beams. It is found that the internal strut exhibits a typical buckling behaviour of imperfect strut which is unstable due to material yielding in its post-buckling range. The UCI is firstly destabilized by the unstable post-buckling behaviour of internal strut and then restabilized when the contribution of external cell becomes dominant in the load resisting mechanism.

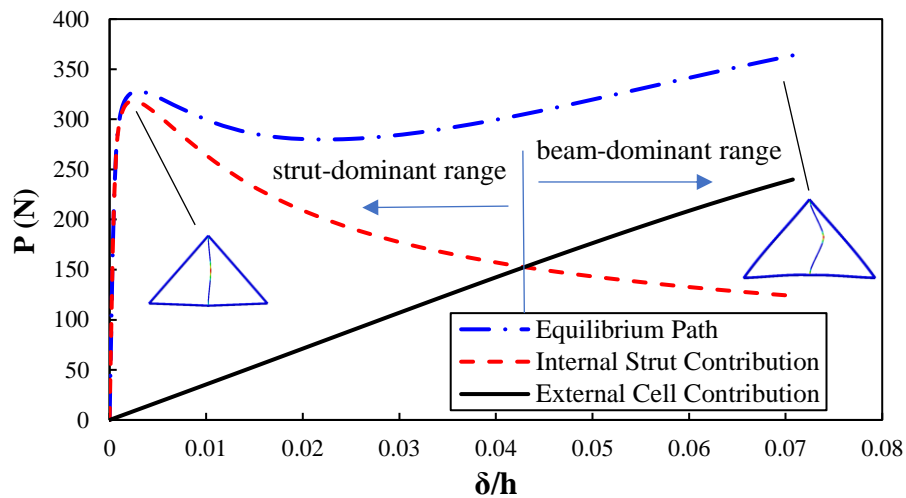


**Figure 2.9** Decomposing of equilibrium path of UCI 1-5

Comparison between the two configurations shows that Configuration 1 will yield a much higher initial stiffness than Configuration 2 (e.g., 4275 N/mm for UCI 1-5 and 515 N/mm for UCI 2-5). This is because the direction of internal strut in Configuration 1 is in line with the direction of external load so that the internal strut will exhibit a typical strut buckling behaviour with an initial stiffness close to its axial stiffness,

whereas the oblique nature of internal struts in Configuration 2 will lower the initial stiffness in comparison with Configuration 1. It is also found that increasing the radius of internal strut will lower  $p_r$ .

### 2.3.5.2 Imperfection sensitivity

Imperfection sensitivity diagrams (**Figure 2.10**) of two UCIs – UCI 1-5 and UCI 2-4 – are constructed for further comparison between the two configurations. The reason of choosing these two UCIs for comparison is that their linear buckling loads  $P^C$  are basically the same (360N for UCI 1-5 and 358.4N for UCI 2-4). Initial geometric imperfection is denoted as  $\varepsilon$  which is the initial deflection at mid span of internal strut(s) while  $l$  is the length of internal strut(s).  $\varepsilon$  increases from 0 to around  $l/250$ . The first finding from **Figure 2.10** is that Configuration 2 is more imperfection insensitive than Configuration 1. The second finding is that the shapes of two imperfection sensitivity curves have different nature with that of Configuration 1 convex to origin and that of Configuration 2 concave to origin. This indicates that the variation of buckling load induced by random imperfection can be further lowered in Configuration 2 by improving the precision of additive manufacturing, however, it is less effective of doing this in Configuration 1 due to its ‘convex’ nature.

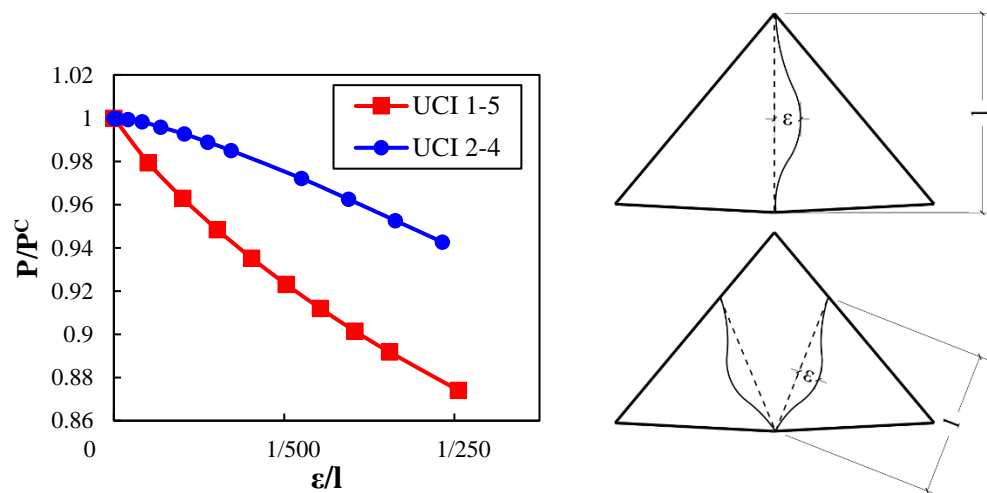


**Figure 2.10** Imperfection sensitivity diagrams

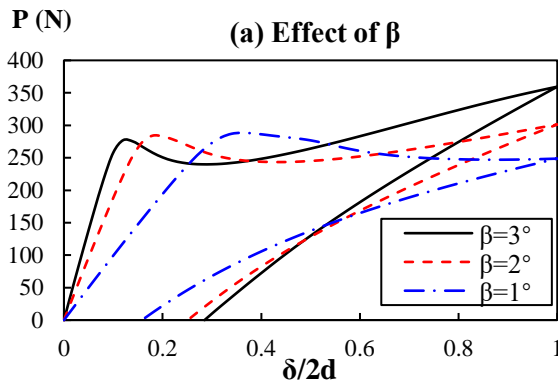
In conclusion, both two configurations are feasible in terms of obtaining snap-through behaviour while Configuration 2 is preferable regarding its less imperfection sensitivity. Thus, in the rest of this thesis, Configuration 2 is employed and further investigated, the abbreviation ‘UCI’ refers only to Configuration 2 unless specifically noted.

### 2.3.6 ‘Designing’ of equilibrium paths

In section 2.3.5, the effect of  $r_i$  on equilibrium path was grasped. However, the effects of  $\beta$ ,  $r$ ,  $\gamma_h$  are still left to be reviewed and will be covered in this section. The results and findings demonstrated that by adjusting geometric and cross-sectional parameters, equilibrium paths of UCIs can be deliberately designed according to practical needs such as objective  $p_r$ , objective buckling load, objective ultimate deformation and energy absorption etc.

#### 2.3.6.1 Effect of $\beta$ , $r$ , $\gamma_h$

To learn the effect of  $\beta$ ,  $r$ ,  $\gamma_h$ , variable-controlling approach is used in three comparative studies, the results are presented in **Figure 2.11 (a), (b), (c)** respectively. In each figure, only the controlled parameter is changed among the three UCI cases while other parameters remain unaltered.  $p_r$  and energy absorption of the three UCIs in **Figure 2.11 (a)** are listed in **Table 2.6**. It should be noted that the horizontal axis in **Figure 2.11 (a)** is no longer  $\delta/h$  but  $\delta/2d$  for visual comparison of recoverability.



\* Other parameters:  $\alpha=50^\circ$ ,  $b=200\text{mm}$ ,  
 $r_i=0.70\text{mm}$ ,  $r=2\text{mm}$ ,  $\gamma_h=1/3$

**Table 2.6**  $p_r$  and energy absorption

$\beta$	$p_r$ (%)	Energy absorption ( $10^{-3}$ J)
$3^\circ$	71.47	2838.29
$2^\circ$	74.86	1721.66
$1^\circ$	84.20	793.822

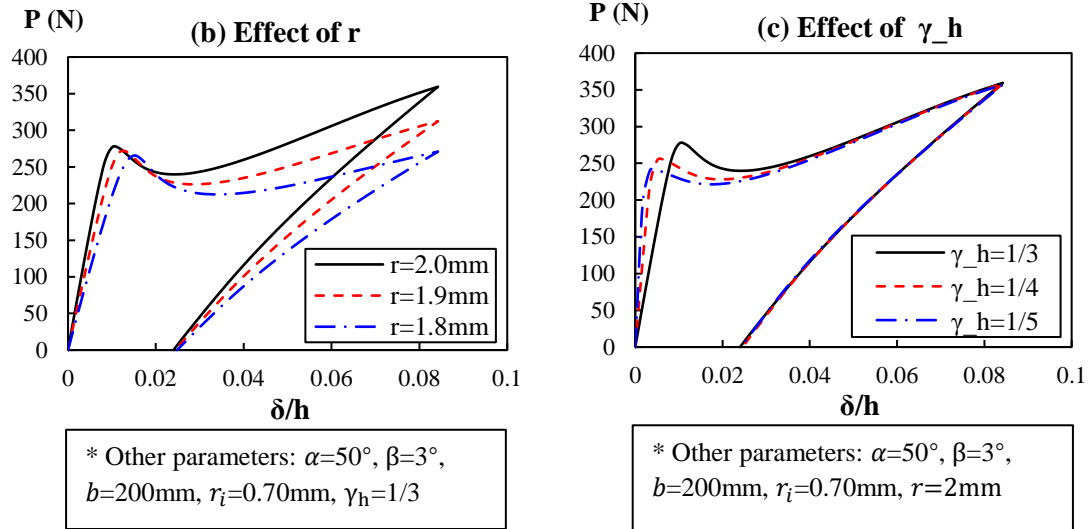


**Figure 2.11** Effect of  $\beta$ ,  $r$ ,  $\gamma_h$

Findings from **Figure 2.11** are threefold: (a) reducing  $\beta$  (equivalent to reducing  $d$ ) will improve recoverability without sacrificing the buckling load, however, it is also shown in **Table 2.6** that the increase in  $pr$  is accompanied by a significant reduction in energy absorption; (b) the tail of equilibrium path will be lifted up by increasing  $r$ . Increasing  $r$  also slightly increase the load magnitude at limit point; (c) the initial stiffness of UCIs could be increased by lowering  $\gamma_h$ .

### 2.3.6.2 Summary

In summary, the designing of equilibrium path can be divided into 4 parts: (a) limit point; (b) tail; (c) initial stiffness; (d) recoverability. The design methods are illustrated in **Figure 2.12**.

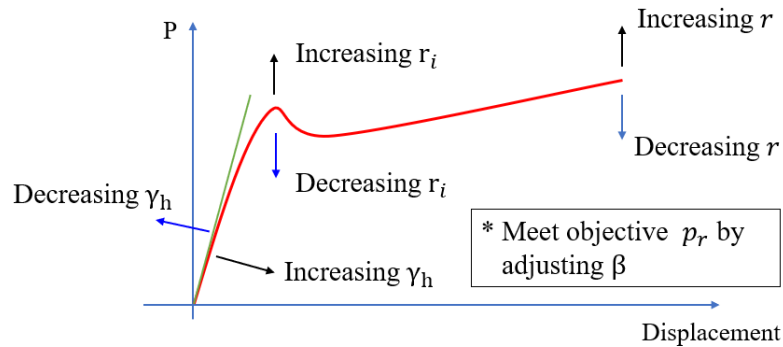


**Figure 2.12** Design diagram

## Chapter 3

### LATTICE

#### 3.1 Introduction

In chapter 2, a thorough investigation was implemented on arrowhead unit cells. This chapter takes a further step from unit cell to 3D lattice structure and seeks for ways of harvesting sequential buckling behaviour in lattices based on the findings from last chapter.

In last chapter unit cells are modelled in 2D planar space, whereas 3D unit cells are needed for the modelling of 3D lattice structure. A 3D unit cell is set as two planar unit cells jointed at right angle, as shown in **Figure 3.1**. A lattice is formed by stacking 3D unit cells together in rows and columns, example of a 3(column) $\times$ 4(row) lattice is shown in **Figure 3.2**.

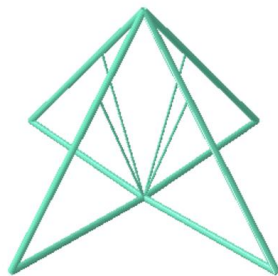


**Figure 3.1** 3D unit cell

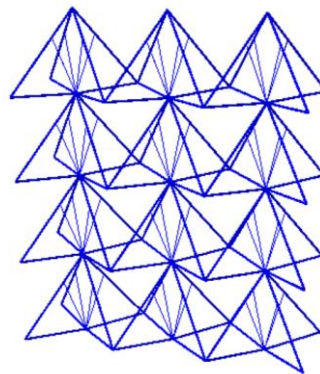


**Figure 3.2** 3 $\times$ 4 lattice

### 3.2 Finite Element Modelling of Lattice

All structural members adopt Quadratic Timoshenko beam element type in 3D space (B32). Theoretical boundary condition is presented in **Figure 3.3 (a)** (shown in 2D plane for simplicity). This boundary condition allows the lateral expansion or shrinkage of lattice. Numerical modelling of this boundary condition is by two steps: (a) coupling the U2 and UR1, UR2, UR3 (vertical displacement and all rotations) of all bottom nodes and all top nodes respectively; (b) fix the middle top node and add a roller support at middle bottom node. It should be noted that the reason why top middle node is fixed instead of pinned is simply for avoiding non-convergence during FE analysis. Since the structure is geometrically symmetric and undergoes symmetric loading, the top middle node is not expected to have any rotation, thus this modification in boundary conditions makes no practical difference but helps converge the FE analysis. **Figure 3.3 (b), (c)** show the boundary conditions of lattice in Abaqus.

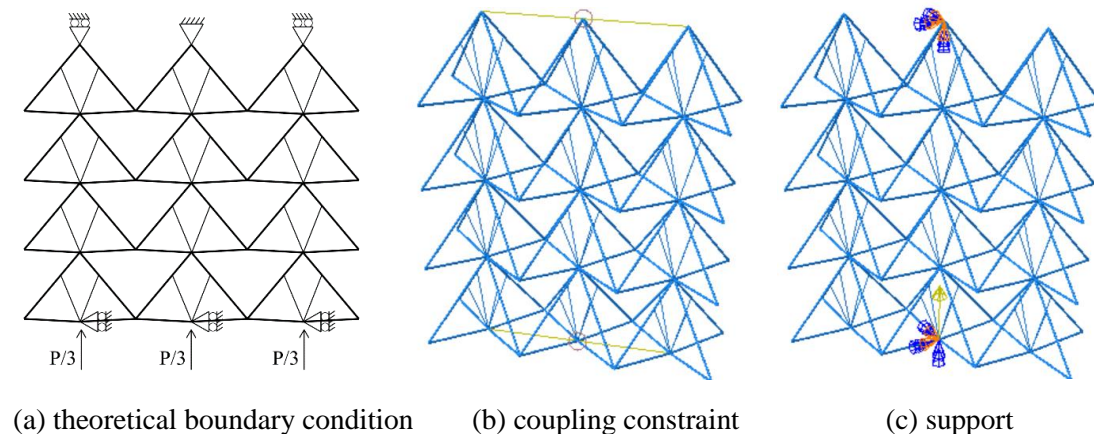


**Figure 3.3** Theoretical and numerical boundary conditions

### 3.3 ‘Lattice Effect’

In an individual unit cell, the left node and right node are free, however, they are jointed with adjacent unit cells in lattice. Thus, deformation of a unit cell in lattice is constrained by adjacent unit cells to some extent. As a result, the required external force to push the unit cell in lattice to a certain magnitude of displacement will be larger than

that for an individual unit cell. This restraining effect is named as ‘lattice effect’ and verified in this section by comparing the equilibrium paths of a 2D individual UCI and a one-row lattice which is composed of ten 2D UCIs (shown in **Figure 3.4**). To make the two cases comparable, the load magnitude for one-row lattice is multiplied by a factor of 1/10 and the factored equilibrium path (curve 1) is plotted with the equilibrium path of 2D UCI (curve 2) together in **Figure 3.5**. It is seen that the tail of curve 1 is higher than that of curve 2. Therefore, to make curve 1 coincide with curve 2, the radius of external beam in lattice needs to be reduced by some amount. To distinguish from  $r$ , this modified radius of external beam in lattice is named as  $r_l$ . In this case, it is confirmed by trial and error that the two curves coincide when  $r_l$  equals to 1.95mm.

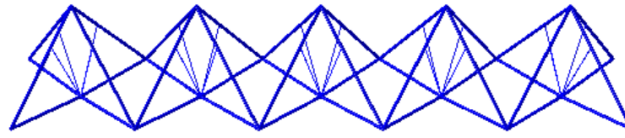


**Figure 3.4** One-row lattice

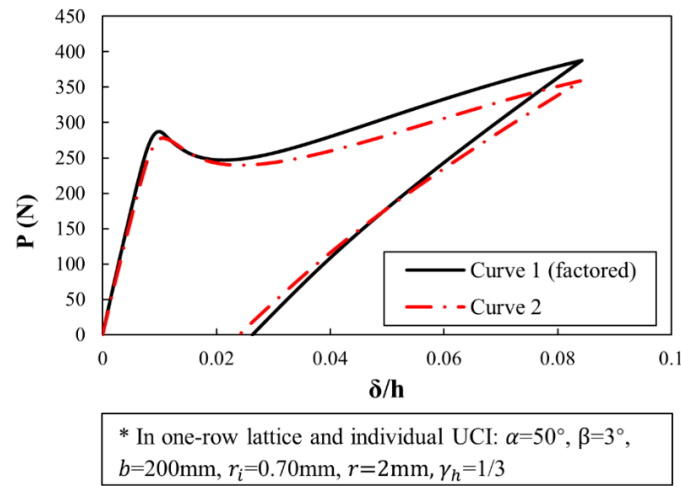


**Figure 3.5** Illustration of ‘lattice effect’

Lattice effect indicates that the design result of UCIs according to section 2.3.6 cannot be directly applied to lattice, modification of  $r$  is required to counteract the lattice effect and thus the mechanical behaviour of individual unit cells can be duplicated into unit cells in lattice.

### 3.4 Lattice with sequential buckling behaviour

#### 3.4.1 Conceptual design

**Figure 3.6** presents a typical equilibrium path of lattice with sequential buckling behaviour which could be regarded as a series of snap buckling of unit cell layers.  $P_i^C$  represents the buckling load of layer  $i$  which corresponds to the  $i^{\text{th}}$  peak on equilibrium path. In order to achieve sequential buckling nature and also ensure a load threshold effect,  $P_i^C$  should meet two requirements: (a)  $P_i^C$  should be progressively increasing such that buckling of layers can be triggered in sequence; (b) the overall increase in  $P_i^C$  should be kept within a relatively small limit. In addition, for a more efficient energy absorption capacity,  $l_i$  is supposed to be as long as possible on condition that the recoverability of lattice is not much sacrificed.

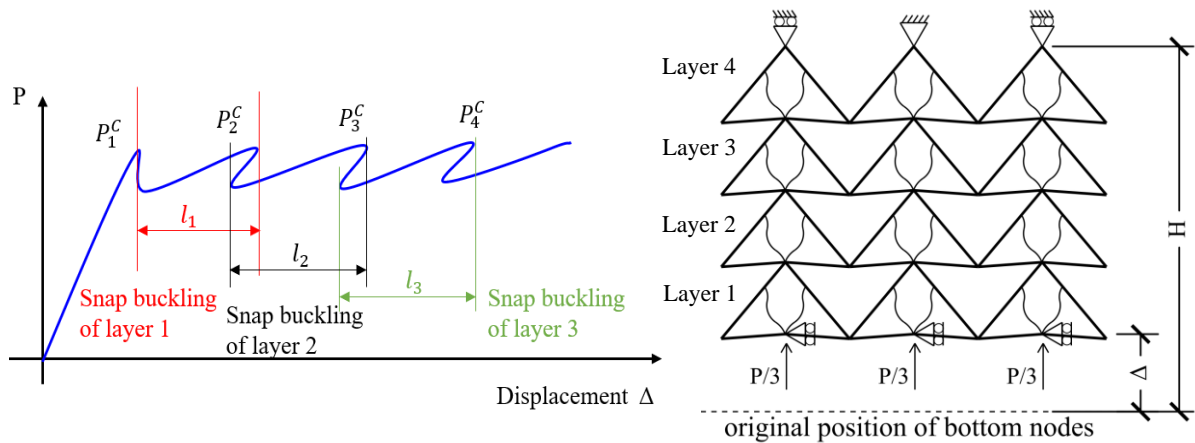


**Figure 3.6** Typical equilibrium path of sequential buckling lattice

The design of sequential buckling lattice can be ultimately broken down to the design of UCI which can be referred to section 2.3.6. **Figure 3.7** shows the desired equilibrium path of UCI which will satisfy the aforementioned three requirements. As a reminder, ‘lattice effect’ should be considered, hence  $r$  which is designed based on individual unit cell needs to be modified to  $r_l$ .

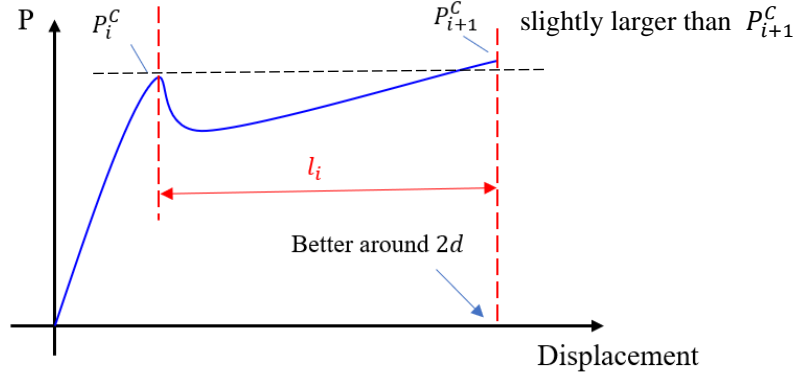


**Figure 3.7** Desired equilibrium path of UCI

### 3.4.2 Design results

Based on principles of conceptual design, two  $3 \times 4$  lattices are designed with their information listed in **Table 3.1**. In lattice 1,  $r_i$  is maintained the same while  $r_{l,i}$  changes among layers while the opposite method is exploited in lattice 2. The value of  $d$  corresponding to  $\beta = 3^\circ$  is 5.24mm. Since  $2d$  is the design ultimate displacement of a single UCI,  $8d$  is set as the design ultimate displacement of a 4-row lattice.

Table 3.1 (a) Lattice 1			(b) Lattice 2		
Position of UCI	$r_{l,i}$	$P_i^C$ (N)	Position of UCI	$r_i$	$P_i^C$ (N)
Layer 1	1.72	277.72	Layer 1	0.68	277.72
Layer 2	1.74	279.26	Layer 2	0.681	279.08
Layer 3	1.76	280.74	Layer 3	0.682	280.47
Layer 4	1.78	282.17	Layer 4	0.683	281.86

\* $r_i=0.68\text{mm}$ ,  $b=200\text{mm}$ ,  
 $\alpha=50^\circ$ ,  $\beta=3^\circ$ ,  $\gamma_h=1/3$

\* $r_{l,i}=1.72\text{mm}$ ,  $b=200\text{mm}$ ,  
 $\alpha=50^\circ$ ,  $\beta=3^\circ$ ,  $\gamma_h=1/3$

### 3.4.3 Numerical results and findings

Equilibrium paths of Lattice 1 and Lattice 2 are presented in **Figure 3.8**, the two curves are cut off at design ultimate displacement which is 41.96mm. To statistically analyse

the two equilibrium paths, the mean and standard deviation of load values within range  $l_i$  are calculated and summarized in **Table 3.2**.

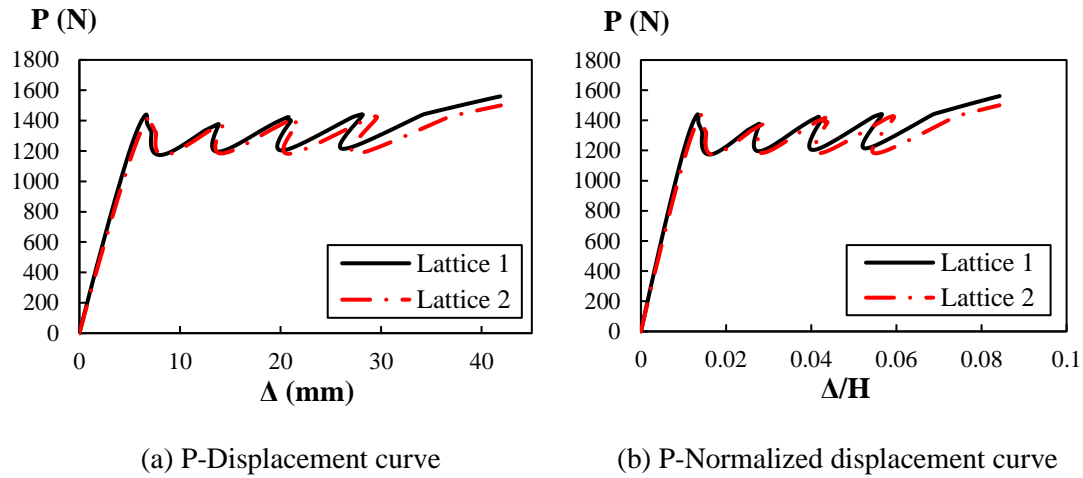


**Figure 3.8** Equilibrium paths of Lattice 1 and Lattice 2

<b>Table 3.2 (a) Lattice 1</b>				<b>(b) Lattice 2</b>			
Range	Mean (N)	Standard deviation	Coefficient of variation	Range	Mean (N)	Standard deviation	Coefficient of variation
$l_1$	1273.259	68.22364	0.053582	$l_1$	1266.065	65.95772	0.052097
$l_2$	1296.206	72.3436	0.055812	$l_2$	1289.001	74.1234	0.057505
$l_3$	1311.669	75.97831	0.057925	$l_3$	1293.346	78.04414	0.060343

It is seen from **Figure 3.8** that for the two lattices, the first peak load is higher than the second one, which is contrary to conceptual design. Besides, there is small fluctuation in load response around the third peak of Lattice 2 because the internal struts in layer 3 do not buckle strictly at the same time, little offset between the buckling of struts is observed. These are probably due to the boundary conditions set up in Abaqus, future study will refine the modelling techniques of boundary conditions to avoid these problems. Lattice 1 and 2 have relatively similar behaviour and are both able to ensure a practically constant level of load resisting capacity in the sequential buckling range. The energy absorption values are 51.2J and 52.6J for Lattice 1 and Lattice 2. The mean values of load and coefficients of variation only slightly increase from  $l_1$  to  $l_3$ , which

proves that both two lattices maintain a good property during the whole sequential buckling process. Another finding is that to keep a progressive but small increase in  $P_i^C$ , the change in  $r_i$  among layers in Lattice 2 should be much less than the change in  $r_{l,i}$  in Lattice 1 because  $P_i^C$  is more sensitive to  $r_i$  rather than  $r_{l,i}$ . Currently, additive manufacturing is not capable of distinguishing a difference in thickness under 20  $\mu\text{m}$  which is the thinnest printable layer thickness, this makes the printing of Lattice 2 unachievable. Thus, Lattice 1 is the preferable option. The percentage of recovery of lattices cannot be directly obtained from FE analysis as the employed Static Riks procedure does not allow unloading step to be defined. Thus, percentage of recovery can only be predicted from the  $p_r$  of UCIs. The UCIs in Lattice 1 and Lattice 2 will give  $p_r$  ranging from 70% -- 75%, thus prediction can be made that percentage of recovery of the two lattices will be within that range too.

It is also worth studying the structural behaviour of the lattices when  $\Delta$  exceeds the design ultimate displacement. **Figure 3.9** shows the extended version of equilibrium paths of Lattice 1 and Lattice 2 which are cut off at the stage where the maximum equivalent plastic strain (PEEQ) of external beams reaches material ultimate strain. It is observed that after sequential buckling range, load-displacement curves start to rise with a low positive stiffness till material failure is witnessed in external beams. For both lattices, the load magnitude at the end of equilibrium path is around 60% larger than the first peak.

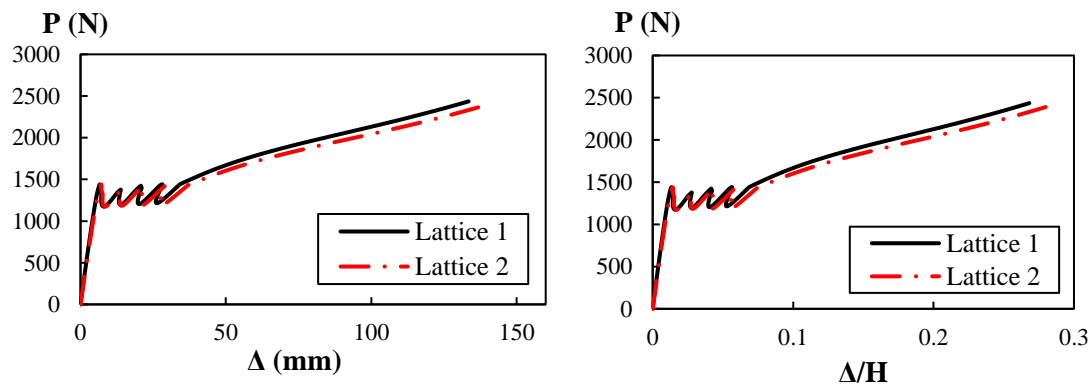


**Figure 3.9** Equilibrium paths (till material failure) of Lattice 1 and Lattice 2

## *Chapter 4*

### **CONCLUSION and RECOMMENDATION**

This study aims at investigating the structural behaviour of recoverable negative stiffness steel lattice structure for the use of structural isolation. The research is organized from part (unit cells) to whole (lattice). It has shown that bare unit cells are not suitable for constituting recoverable lattice, whereas unit cells with internal strut(s) are proved to be applicable. Further investigation has demonstrated that the equilibrium paths of unit cells are tailorable by adjusting critical parameters. Based on numerical results and findings of unit cells, steel lattices with sequential buckling behaviour have been designed and analysed numerically. It has shown that the designed lattice is able to maintain its desirable property during sequential buckling process and a predicted 70-75% of recovery is met corresponding to an 8% normalized deformation.

This study is certainly not exhaustive and recommended future work can be organized as threefold: firstly, numerical modelling techniques for lattice structure is required to be refined in order to simulate practical conditions; secondly, possible methods should be searched for to lower the structural stiffness after the design ultimate displacement is exceeded; thirdly, experimental work should be carried out to validate the numerical results and also give indications on updating numerical modelling techniques.

## References

Bažant, Z. P. (2000) Structural stability. *International Journal of Solids and Structures*. 37 (1-2), 55-67. Available from: doi:10.1016/S0020-7683(99)00078-5.

Carrella, A., Brennan, M. J. & Waters, T. P. (2007) Static analysis of a passive vibration isolator with quasi-zero-stiffness characteristic. *Journal of Sound and Vibration*. 301 (3-5), 678-689. Available from: doi: 10.1016/j.jsv.2006.10.011.

Cheng, Y., Li, J., Qian, X. & Rudykh, S. (2021) 3D printed recoverable honeycomb composites reinforced by continuous carbon fibers. *Composite Structures*. 268 113974. Available from: doi: 10.1016/j.matdes.2017.10.028.

Deng, F., Nguyen, Q. & Zhang, P. (2020) Multifunctional liquid metal lattice materials through hybrid design and manufacturing. *Additive Manufacturing*. 33 101117. Available from: doi: 10.1016/j.addma.2020.101117.

Frazier, W. E. (2014) Metal Additive Manufacturing: A Review. *Journal of Materials Engineering and Performance*. 23 (6), 1917-1928. Available from: doi: 10.1007/s11665-014-0958-z.

Gibson, L. J., and Ashby, M. F. (1999). *Cellular Solids: Structure and Properties, 2nd Edn*. Cambridge Solid State Science Series. Cambridge: Cambridge University Press.

Großmann, A., Gosmann, J. & Mittelstedt, C. (2019) Lightweight lattice structures in selective laser melting: Design, fabrication and mechanical properties. *Materials Science and Engineering: A*. 766 138356. Available from: doi: 10.1016/j.msea.2019.138356.

Hatamleh, M. I., Barrios, C. A., Ren, Y., Zhang, R., Nambiar, V. V., Williams, A., Shah, P., Guyan, A., Lund, B., Lu, H. & Voit, W. (2021) Structural response of 3D-printed rubber lattice structures under compressive fatigue. *MRS Communications*. 11 (2), 168-172. Available from: doi: 10.1557/s43579-021-00012-4.

Hu, N. & Burgueño, R. (2015) Buckling-induced smart applications: recent advances and trends. *Smart Materials and Structures*. 24 (6), 063001. Available from: doi: 10.1088/0964-1726/24/6/063001.

Hunt, G. W., Lord, G. J. & Champneys, A. R. (1999) Homoclinic and heteroclinic orbits underlying the post-buckling of axially-compressed cylindrical shells. *Computer Methods in Applied Mechanics and Engineering*. 170 (3-4), 239-251. Available from: doi: 10.1016/S0045-7825(98)00197-2.

McKown, S., Shen, Y., Brookes, W. K., Sutcliffe, C. J., Cantwell, W. J., Langdon, G. S., Nurick, G. N. & Theobald, M. D. (2008) The quasi-static and blast loading response of lattice structures. *International Journal of Impact Engineering*. 35 (8), 795-810. Available from: doi: 10.1016/j.ijimpeng.2007.10.005.

Qiu, J., Lang, J. H. & Slocum, A. H. (2004) A Curved-Beam Bistable Mechanism. *Journal of Microelectromechanical Systems*. 13 (2), 137-146. Available from: doi: 10.1109/JMEMS.2004.825308.

Reis, P. M. (2015) A Perspective on the Revival of Structural (In)Stability With Novel Opportunities for Function: From Buckliphobia to Buckliphilia. *Journal of Applied Mechanics*. 82 (11). Available from: doi: 10.1115/1.4031456.

Riks, E. (1979) An incremental approach to the solution of snapping and buckling problems. *International Journal of Solids and Structures*. 15 (7). Available from: doi: 10.1016/0020-7683(79)90081-7.

Wadee, M. A. & Gardner, L. (2012) Cellular buckling from mode interaction in I-beams under uniform bending. *Proceedings of the Royal Society A: Mathematical, Physical and Engineering Sciences*. 468 (2137), 245-268. Available from: doi: 10.1098/rspa.2011.0400.

Wadee, M. A. & Bai, L. (2014) Cellular buckling in I-section struts. *Thin-Walled Structures*. 81 89-100. Available from: doi: 10.1016/j.tws.2013.08.009.

Wadee, M. A. & Farsi, M. (2014) Cellular buckling in stiffened plates. *Proceedings of the Royal Society A: Mathematical, Physical and Engineering Sciences*. 470 (2168), 20140094. Available from: doi: 10.1098/rspa.2014.0094.

Wadee, M. A., Phillips, A. T. M. & Bekele, A. (2020) Effects of Disruptive Inclusions in Sandwich Core Lattices to Enhance Energy Absorbency and Structural Isolation Performance. *Frontiers in Materials*. 7. Available from: doi: 10.3389/fmats.2020.00134.

Wadley, H., Dharmasena, K., Chen, Y., Dudt, P., Knight, D., Charette, R. & Kiddy, K. (2008) Compressive response of multilayered pyramidal lattices during underwater shock loading. *International Journal of Impact Engineering*. 35 (9), 1102-1114. Available from: doi: 10.1016/j.ijimpeng.2007.06.009.

Zhang, R., Gardner, L., Meng, X., Buchanan, C., Matilainen, V. P., Piili, H., & Salminen, A. (2021). Optimization and compressive testing of additively manufactured stainless steel corrugated shells. *Eurosteel 2021*, Sheffield, UK.